Journal of Fluids and Structures (1997) **11,** 857–872

INFLUENCE OF SEPARATION ON SOUND GENERATED BY VORTEX-STEP INTERACTION

M. S. Howe

College of Engineering, Boston University, 110 Cummington Street Boston, MA 02215, U.S.A.

(Received 15 April 1997 and in revised form 22 August 1997)

An analysis of the sound produced when a line vortex interacts at low Mach number with forward or backward facing steps is made. The radiation is dominated by an aeroacoustic dipole whose strength is equal to the unsteady drag on the step. The drag is determined by the vorticity distribution, and a correct estimate of the sound must therefore include contributions from vorticity in the separated flow induced by the vortex. The separation is modelled by assuming that the shed vorticity rolls up into a concentrated core, fed by a connecting sheet from the edge of the step of negligible circulation. The motion everywhere is irrotational except at the impinging vortex and the separation core, and the trajectory of the core is governed by an emended Brown & Michael equation. For large steps it is found that estimates of the generated sound that neglect separation are typically an order of magnitude too large. The sound levels predicted for small steps with and without separation are of comparable magnitudes, although the respective *phases* are different. *Turbulent* flow over a step frequently involves separation and large surface pressure fluctuations at reattachment zones. The results of this paper suggest that numerical schemes for determining the noise generated by turbulent flow over a step must take proper account of "forcing" of the separation region by the impinging turbulence and of vorticity production via the no-slip condition.

1. INTRODUCTION

Boundary layer turbulence and other flow inhomogeneities can promote unsteady separation from structural irregularities, such as rivet heads, lap-joints, cutouts, etc. The unsteady drag exerted on the irregularity is equivalent to a localized aeroacoustic dipole, and is responsible for the production of both sound and structural vibration. Lap-joints (or "skin steps") occur at junctions of neighbouring panels on an aircraft fuselage, and are a possible source of boundary-layer-generated interior cabin noise, either because they enhance downstream wall pressure fluctuations and drive vibrations of the cabin walls, or because the drag dipole is a direct source of sound and vibration (Efimtsov 1996; Howe 1997).

Irregularities in the form of forward or backward facing steps have been studied extensively (Bradshaw & Wong 1972; Moss & Baker 1980; Chandrsuda & Bradshaw 1981; Eaton & Johnston 1981; Farabee & Casarella 1984, 1986, 1988) because their free shear layers possess well-defined separation and reattachment zones. More generally, reattachment occurs downstream of a stagnation point, and is a region of high-fluctuating wall

0889-9746/97/080857 + 16 $25.00/fl970113

pressure, where free shear layer eddies bifurcate into upstream and downstream travelling components (Bradshaw & Wong 1972). According to Farabee & Casarella (1984, 1986), low Mach number turbulent wall pressures at reattachment for backward and forward facing steps (with step heights comparable to the boundary-layer thickness) are, respectively, about 5 and 10 times larger than the smooth wall boundary-layer pressures. The wall pressure must ultimately revert to that of a smooth wall boundary layer, but differences have been observed at distances as large as 72 step heights downstream of the step.

The large changes in the boundary-layer structure at a step must be carefully modelled to obtain accurate estimates of the sound produced by the boundary-layer–step interaction. For example, in low-to-moderate Mach number flows, the unsteady drag (which is the dipole source strength) is determined by the vorticity distribution near the step (Howe 1989*a*, 1995), which includes vorticity in the impinging flow together with any produced by the interaction and "trapped" in the recirculating separation bubble. Hitherto, theoretical predictions of the generated sound [e.g. Conlisk & Veley (1985); Dhanak & Gundlapalli (1992); Howe (1989*b*, 1997)] have tended to ignore separation and vorticity production. Conlisk & Veley (1985) and Dhanak & Gundlapalli (1992) represented the impinging inhomogeneous flow by an assembly of line (or *point*) vortices, whose motions over a large step (comparable in size to the boundary-layer thickness) were determined from inviscid equations of motion. Howe (1989*b*, 1997) considered "small" steps, and calculated the sound as a by-product of the scattering of the boundary-layer pressure field, which was assumed to be *frozen* during convection over the step.

In this paper, we assess the accuracy of these inviscid approximations from an analysis of the interaction of a single line vortex with a forward or backward facing step. Separation is modelled by assuming that the vorticity shed during the interaction rolls up into a concentrated core, which grows in strength by the passage of continuously shed vorticity along a connecting sheet from the edge of the step. The motion is irrotational everywhere except at the impinging vortex and the core of the shed vorticity, and the trajectory of the core is determined by the emended Brown & Michael equation (Brown & Michael 1954, 1955; Howe 1996). For large steps, it is concluded that estimates of the sound that neglect separation are typically an order of magnitude too large. This is because the calculated drag on the step is greatly overestimated when the potential theory singularity at the edge of the step is not suppressed by vortex shedding. For small steps, predicted sound levels with and without separation are of comparable magnitudes, but exhibit large differences in *phase*.

The aerodynamic sound problem is formulated in Section 2 for low Mach, self-induced vortex motion over forward or backward facing steps on a plane wall. Numerical predictions of the sound are presented in Section 3.

2. THE AERODYNAMIC SOUND PROBLEM

2.1. Formulation

A line vortex of circulation $\Gamma_0 > 0$ is in translational motion adjacent to a rigid wall. The vortex is parallel to the z-axis of the rectangular coordinate system (x, y, z) and the wall is parallel to the plane $y = 0$, except for a "vertical" step of height h, whose foot coincides with the z-axis. To fix ideas, consider the forward-facing step illustrated schematically in Figure 1, where the coordinate origin is at O, and the fluid and vortex lie in the region $y \geqslant 0$ "above" the wall.

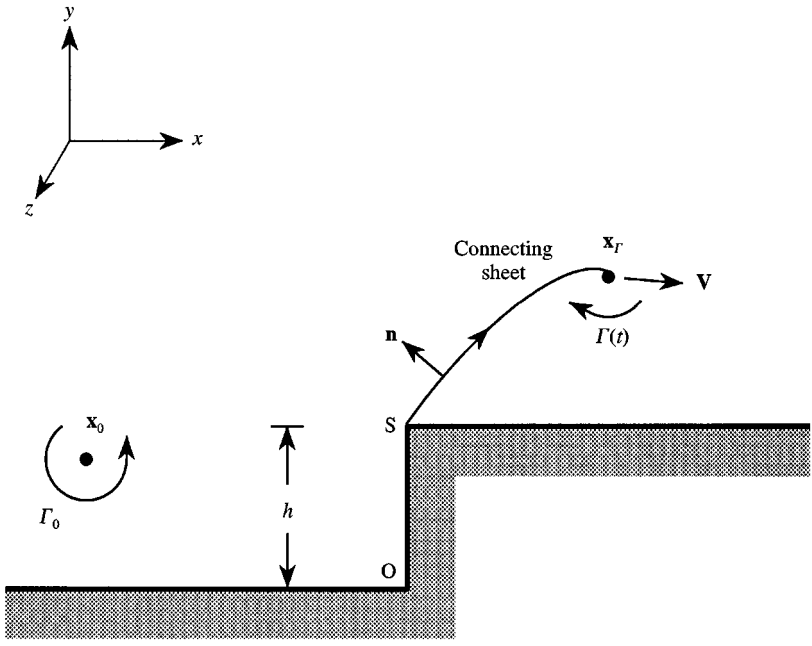

Figure 1. Configuration of the incident and shed vortices for a forward-facing step.

In the undisturbed state the fluid is at rest, and is inviscid except that vortex shedding is permitted from the right-angled edge S of the step to remove the singular velocity and pressure that would otherwise occur. Vortex shedding is uniform along the step, and is modelled by a line vortex of variable strength $\Gamma(t)$ (t denoting time) whose axis intersects the plane $z = 0$ at $(x, y) = \mathbf{x}_\Gamma(t)$, and translates at velocity $\mathrm{d}\mathbf{x}_\Gamma/\mathrm{d}t \equiv \mathbf{V}$. The vortex strength increases as shed vorticity is continuously "fed" along a connecting sheet from S. The circulation of the connecting sheet is assumed to be negligible compared to Γ. This model of vortex shedding, involving a time-dependent core Γ containing all of the shed vorticity, includes a spurious pressure jump across the connecting sheet, which is countered by requiring the translational velocity $\mathbf{V}$ to be different from the fluid velocity $\mathbf{v}$ at the core (Brown & Michael 1954, 1955). $\Gamma(t)$ is assumed to vary monotonically until the vortex is finally "released" from S when $\mathrm{d}\Gamma/\mathrm{d}t$ changes sign. The "free" vortex (with no connecting sheet) then proceeds to convect with the fluid at velocity $\mathbf{v}$, and a new vortex is released from S. In the present discussion, $\mathrm{d}\Gamma/\mathrm{d}t$ turns out to be one-signed during the dominant interaction of the incident vortex Γ_0 with the step.

Let (x_0, y_0) be the position of the incident vortex in the plane $z = 0$ at time t. The vorticity $\boldsymbol{\omega}$ can then be written

$$\boldsymbol{\omega} = \boldsymbol{\Omega}_0 + \boldsymbol{\Omega},$$

$$\boldsymbol{\Omega}_0 = \Gamma_0 \mathbf{k}\delta(x - x_0(t))\delta(y - y_0(t)),$$

$$\boldsymbol{\Omega} = \Gamma(t)\mathbf{k}\delta(x - x_\Gamma(t))\delta(y - y_\Gamma(t)), \tag{2.1}$$

where $\mathbf{k} = (0, 0, 1)$ is a unit vector in the z-direction (out of the plane of the paper in Figure 1). For an ideal fluid the momentum equation is

$$\frac{\partial \mathbf{v}}{\partial t} + \nabla\left(\int \frac{\mathrm{d}p}{\rho} + \frac{1}{2}\mathbf{v}^2\right) = -\boldsymbol{\omega} \wedge \mathbf{v} + \frac{\mathbf{F}}{\rho}, \tag{2.2}$$

where p and ρ are, respectively, the pressure and density, and for two-dimensional motion $\mathbf{v} = (u, v, 0)$. $\mathbf{F}$ is the distributed force

$$\mathbf{F} = \rho\boldsymbol{\Omega} \wedge (\mathbf{v} - \mathbf{V}) - \rho\frac{\mathrm{d}\Gamma}{\mathrm{d}t}\mathbf{n}\delta(x_\perp)H(s_\Gamma - s), \quad s > 0, \tag{2.3}$$

where $x_\perp$ is distance from the connecting sheet measured in the direction of the local normal $\mathbf{n}$ of Figure 1, s_Γ is the length of the sheet (between S and Γ), and s is distance measured along the sheet from S. The first term on the righthand side of equation (2.3) is concentrated at the core of the shed vortex, and is equal and opposite to the Joukowski lift on Γ which arises when $\mathbf{V} \neq \mathbf{v}$; the second term represents the pressure force across the connecting sheet (Howe 1996).

2.2. Equations of Motion of the Vortices

The incident vortex is "free" and translates at the fluid velocity $\mathbf{v}(x, y, t)$ evaluated at its core,

$$\frac{\mathrm{d}\mathbf{x}_0}{\mathrm{d}t} = \mathbf{v}(x_0, y_0, t). \tag{2.4}$$

This velocity is calculated according to potential flow theory, and consists of a contribution from the *images* of Γ_0 in the rigid wall and from the shed vortex Γ and its images.

Brown & Michael (1954, 1955) obtain the equation of motion of the shed vortex by requiring the net force exerted on the fluid by the distribution $\mathbf{F} = (F_x, F_y)$ to vanish. Performing the integration $\int F_y\,\mathrm{d}x/\mathrm{d}y$ for the y-component of equation (2.3), this condition yields

$$\frac{\mathrm{d}x_\Gamma}{\mathrm{d}t} + \frac{x_\Gamma}{\Gamma}\frac{\mathrm{d}\Gamma}{\mathrm{d}t} = u(x_\Gamma, y_\Gamma, t). \tag{2.5}$$

For the horizontal (x-) component, however, it is not sufficient to require $\int F_x\,\mathrm{d}x\,\mathrm{d}y = 0$, since the surface reaction to the remaining unbalanced couple ($\int \mathbf{x} \wedge \mathbf{F}\,\mathrm{d}x\,\mathrm{d}y$) produces an additional unsteady drag on the step. In this case, it is necessary to impose the condition that the *net* horizontal force on the fluid due to $\mathbf{F}$ and its *interaction with the step* is zero. This is done by requiring the path of the shed vortex to satisfy (Howe 1996)

$$\int \mathbf{F} \cdot \nabla X\,\mathrm{d}x\,\mathrm{d}y = 0, \tag{2.6}$$

where $X \equiv X(x, y)$ is a harmonic function that depends only on the shape of the step, and is equal to the velocity potential of ideal, incompressible flow past the step that has unit speed in the x-direction at large distances from the step. Equation (2.6) is expressed in differential form by making use of the Cauchy–Riemann relations

$$\partial X/\partial x = \partial \Psi/\partial y, \qquad \partial X/\partial y = -\partial \Psi/\partial x, \tag{2.7}$$

where Ψ is the stream-function conjugate to X. When $\Psi \equiv 0$ on the wall, equation (2.6) is equivalent to

$$\frac{\mathrm{d}\mathbf{x}_\Gamma}{\mathrm{d}t}\cdot\nabla\Psi + \frac{\Psi}{\Gamma}\frac{\mathrm{d}\Gamma}{\mathrm{d}t} = \mathbf{v}\cdot\nabla\Psi, \qquad (x, y) = (x_\Gamma, y_\Gamma). \tag{2.8}$$

This equation is reduced to the following simplified form by subtracting equation (2.5) multiplied by $\partial\Psi/\partial x$:

$$\frac{\mathrm{d}y_\Gamma}{\mathrm{d}t} + \frac{(\Psi - x_\Gamma\Psi_x)}{\Psi_y}\frac{1}{\Gamma}\frac{\mathrm{d}\Gamma}{\mathrm{d}t} = v(x_\Gamma, y_\Gamma, t), \tag{2.9}$$

where $(\Psi_x, \Psi_y) = (\partial\Psi/\partial x, \partial\Psi/\partial y)$.

2.3. The Aerodynamic Sound

At low Mach numbers, the production of aerodynamic sound by the vorticity and force distribution on the right-hand side of Equation (2.2) is governed by the inhomogeneous wave equation (Howe 1975, 1996)

$$(\partial^2/c_0^2\partial t^2 - \nabla^2)\mathscr{B} = \mathrm{div}(\boldsymbol{\omega}\wedge\mathbf{v}) - \mathrm{div}(\mathbf{F}/\rho_0) \tag{2.10}$$

where $\mathscr{B} \equiv p/\rho_0 + \frac{1}{2}\mathbf{v}^2$ (the total *enthalpy* in isentropic flow) and ρ_0, c_0 are, respectively, the mean density and sound speed. In irrotational regions, the motion can be described by a velocity potential $\phi(\mathbf{x}, t)$, and $\mathscr{B} \equiv -\partial\phi/\partial t$. Thus, at large distances from the step, where the perturbed motion is small, the pressure $p \approx \rho_0\mathscr{B}$, and the solution of equation (2.10) can be expressed in the form

$$p(\mathbf{x}, t) \approx -\int(\rho_0\boldsymbol{\omega}\wedge\mathbf{v} - \mathbf{F})(\mathbf{y}, \tau)\cdot\frac{\partial G}{\partial\mathbf{y}}(\mathbf{x}, \mathbf{y}, t-\tau)\,\mathrm{d}^3\mathbf{y}\,\mathrm{d}\tau, \quad \mathbf{y} = (x', y', z'), \tag{2.11}$$

where the integration is over the fluid and all times τ. In this formula, $G(\mathbf{x}, \mathbf{y}, t-\tau)$ is the Green's function with outgoing wave behaviour that has vanishing normal derivative on the wall, i.e. the solution of equation (2.10) when the right-hand side is replaced by $\delta(\mathbf{x}-\mathbf{y})\delta(t-\tau)$.

The characteristic wavelength of the generated sound is much larger than the step height h when the Mach number is small, and G is then well represented by the *compact* approximation (Howe 1989b).

$$G(\mathbf{x}, \mathbf{y}, t-\tau) \approx \frac{\delta(t-\tau-|\mathbf{x}-\mathbf{Y}|/c_0)}{4\pi|\mathbf{x}-\mathbf{Y}|} + \frac{\delta(t-\tau-|\mathbf{x}-\bar{\mathbf{Y}}|/c_0)}{4\pi|\mathbf{x}-\bar{\mathbf{Y}}|}, \quad |\mathbf{x}|\to\infty,$$

$$\mathbf{Y} = (X(x', y'), y', z'), \qquad \bar{\mathbf{Y}} = (X(x', y'), -y', z'). \tag{2.12}$$

To use this formula in the general solution (2.11), it will be assumed that the effective source region lies within the finite span $-\frac{1}{2}\ell < z < \frac{1}{2}\ell$, where ℓ is small compared to the dominant acoustic wavelengths. This approximation is not essential to the following discussion, but corresponds more closely to conditions in practical problems, where the radiation spreads three dimensionally rather than cylindrically. When end effects (from $z = \pm\frac{1}{2}\ell$) of the source distributions are ignored, the only nontrivial contributions to the

radiation are supplied by the following approximation to G, obtained by taking the first term in the expansion of equation (2.12) in powers of the retarded source position:

$$G(\mathbf{x}, \mathbf{y}, t-\tau) \approx \frac{X(x', y')\cos\theta}{2\pi c_0 |\mathbf{x}|}\, \delta'(t-\tau-|\mathbf{x}|)/c_0), \tag{2.13}$$

where the prime on the δ-function denotes differentiation with respect to time, and $\theta = \cos^{-1}(x/|\mathbf{x}|)$ is the angle between the observer direction in the acoustic far field and the x-axis.

When this expression is substituted into the general solution (2.11), it follows from equation (2.6) and the Cauchy–Riemann equations (2.7) that the contribution from $\mathbf{F}$ vanishes identically, and that the acoustic pressure can be written

$$p(\mathbf{x}, t) \approx \frac{\rho_0 \ell \cos\theta}{2\pi c_0 |\mathbf{x}|} \frac{\mathrm{d}}{\mathrm{d}t} \left[(\Gamma_0 \mathbf{v}\cdot\nabla\Psi)_{\mathbf{x}_0(t)} + (\Gamma(t)\mathbf{v}\cdot\nabla\Psi)_{\mathbf{x}_\Gamma(t)} \right]_{t-|\mathbf{x}|/c_0}, \qquad |\mathbf{x}| \to \infty, \tag{2.14}$$

where the notation implies that the terms in the square braces are evaluated at the retarded time $t - |\mathbf{x}|/c_0$.

3. NUMERICAL RESULTS

3.1. Vortex Trajectories

The vortex paths are determined by equation (2.4) for the incident vortex Γ_0 and equations (2.5) and (2.9) for the shed vortex Γ. The irrotational velocity $\mathbf{v}$ is computed in the usual way, by introducing the dimensionless complex variable

$$Z = \frac{x}{h} + \mathrm{i}\frac{y}{h},$$

and transforming the fluid region above the step onto the upper-half of the complex ζ-plane. This is accomplished by the mapping

$$Z = \frac{1}{\pi}\{\sqrt{\zeta^2-1} \mp \ln(\zeta + \sqrt{\zeta^2-1})\} + \frac{\mathrm{i}}{2}(1 \pm 1), \qquad \mathscr{I}m\,\zeta \geqslant 0, \tag{3.1}$$

where, here and henceforth, upper/lower signs are to be taken, respectively, for the forward/backward facing step. The foot of the step O maps into the point $\zeta = \mp 1$, and the top S maps into $\zeta = \pm 1$.

Let ζ_0 and ζ_Γ denote the respective images in the ζ-plane of the incident and shed vortices. At low Mach numbers, when the step is acoustically compact, the motion near the step may be regarded as incompressible, with complex potential

$$w = \frac{-\mathrm{i}\Gamma_0}{2\pi}[\ln(\zeta-\zeta_0) - \ln(\zeta-\zeta_0^*)] + \frac{-\mathrm{i}\Gamma}{2\pi}[\ln(\zeta-\zeta_\Gamma) - \ln(\zeta-\zeta_\Gamma^*)], \tag{3.2}$$

where the asterisk denotes the complex conjugate. The instantaneous value of $\Gamma(t)$ is determined from the Kutta condition that $\mathrm{d}w/\mathrm{d}z$ should be finite at S, which is satisfied provided $\mathrm{d}w/\mathrm{d}\zeta \to 0$ as $\zeta \to \pm 1$, respectively, for forward and backward facing steps. This yields

$$\frac{\Gamma(t)}{\Gamma_0} = -\left|\frac{1 \mp \zeta_\Gamma}{1 \mp \zeta_0}\right|^2 \left(\frac{\zeta_0 - \zeta_0^*}{\zeta_\Gamma - \zeta_\Gamma^*}\right), \tag{3.3}$$

which implies that Γ and Γ_0 always have opposite signs.

The velocity $\mathbf{v}(x_0, y_0, t)$ of the incident vortex, on the right-hand side of equation (2.4), is calculated from the velocity potential (3.2) by first excluding the free-field self-potential $(-\mathrm{i}\Gamma_0/2\pi)\ln(Z - Z_0)$, where $Z_0 = x_0/h + \mathrm{i}y_0/h$. In the ζ-plane, equation (2.4) is equivalent to

$$\frac{\mathrm{d}\zeta_0}{\mathrm{d}T} = -\mathrm{i}/\mathscr{F}(\zeta_0)\left[\left(\frac{1}{\zeta_0^* - \zeta_0} + \frac{1}{2(\zeta_0^2 - 1)^*}\right) - \frac{\Gamma}{\Gamma_0}\left(\frac{1}{\zeta_0^* - \zeta_\Gamma^*} - \frac{1}{\zeta_0^* - \zeta_\Gamma}\right)\right], \tag{3.4}$$

where

$$T = \frac{\pi\Gamma_0 t}{2h^2}, \qquad \mathscr{F}(\zeta) = \sqrt{\frac{\zeta \pm 1}{\zeta \mp 1}}. \tag{3.5}$$

Similarly, the velocity components $u(x_\Gamma, y_\Gamma, t)$ and $v(x_\Gamma, y_\Gamma, t)$ in the equations of motion (2.5) and (2.9) of Γ are evaluated from equation (3.2) by excluding $(-\mathrm{i}\Gamma/2\pi)\ln(Z - Z_\Gamma)$, $Z_\Gamma = x_\Gamma/h + \mathrm{i}y_\Gamma/h$. The stream function $\Psi = \mathscr{I}m(h\zeta/\pi)$, so that, in the ζ-plane, ζ_Γ satisfies

$$\frac{\mathrm{d}\zeta_\Gamma}{\mathrm{d}T} + \frac{\mathscr{F}(\zeta_\Gamma)}{\mathscr{R}e[\mathscr{F}(\zeta_\Gamma)]}\left(\mathrm{i}\mathscr{I}m(\zeta_\Gamma) + \pi\mathscr{R}e(Z_\Gamma)\mathscr{F}^*(\zeta_\Gamma)\right)\frac{1}{\Gamma}\frac{\mathrm{d}\Gamma}{\mathrm{d}T}$$

$$= -\mathrm{i}\,|\mathscr{F}(\zeta_\Gamma)|\left[\frac{\Gamma}{\Gamma_0}\left(\frac{1}{\zeta_\Gamma^* - \zeta_\Gamma} + \frac{1}{2(\zeta_\Gamma^2 - 1)^*}\right) - \left(\frac{1}{\zeta_\Gamma^* - \zeta_0^*} - \frac{1}{\zeta_\Gamma^* - \zeta_0}\right)\right], \tag{3.6}$$

where $\mathscr{R}e(Z_\Gamma)$ on the left-hand side is given in terms of ζ_Γ by equation (3.1).

Equations (3.3)–(3.6) are solved numerically by assigning a large and negative initial value to $\mathscr{R}e(\zeta_0)$ and adjusting the corresponding value of $\mathscr{I}m(\zeta_0)$ to make the stand-off distance d, say, of the vortex Γ_0 from the wall equal to some prescribed initial value. The starting value of ζ_Γ is taken at some point close to the image $\zeta = \pm 1$ of the step top S; the precise location depends on the integration step length, but does not critically affect the solution, since Γ is very small when the shed vortex is close to S, and the starting errors rapidly become negligible as the solution builds up with the approach of Γ_0 to the step. A fourth-order Runge–Kutta procedure was used; the equations form a robust system and no difficulty was experienced in achieving convergence.

3.2. Acoustic Pressure

The acoustic pressure (2.14) may now be expressed in the form

$$p(\mathbf{x}, t) \approx 8\pi^3\rho_0 U^2 M\left(\frac{d}{h}\right)^3 \frac{\ell\cos\theta}{|\mathbf{x}|}\frac{\mathrm{d}}{\mathrm{d}T}\left[\mathscr{I}m\left(\frac{\mathrm{d}\zeta_0}{\mathrm{d}T}\right) + \frac{\Gamma(T)}{\Gamma_0}\mathscr{I}m\left(\frac{\mathrm{d}\bar{\zeta}_\Gamma}{\mathrm{d}T}\right)\right]_{t-|\mathbf{x}|/c_0},$$

$$M = \frac{U}{c_0}, \tag{3.7}$$

where $\mathrm{d}\bar{\zeta}_\Gamma/\mathrm{d}T$ is proportional to the fluid velocity at the core of the shed vortex Γ (which is the same as the vortex translation velocity $\mathbf{V}$ only when $\mathrm{d}\Gamma/\mathrm{d}t = 0$) and is equal to the right-hand side of equation (3.6) evaluated at the retarded position of Γ. The velocity $U \equiv \Gamma_0/4\pi d$ is the initial translational velocity (which is parallel to the wall) of the incident vortex before its motion is affected by the step. The acoustic pressure is proportional to $\rho_0 U^2 M$, which is typical of an aeroacoustic source of *dipole* type; the dipole strength is just the unsteady drag exerted on the step during the interaction.

3.3. The Forward-Facing Step

Consider first the hypothetical case of vortex motion and acoustic radiation in the *absence* of vortex shedding (Conlisk & Veley 1985; Dhanak & Gundlapalli 1992). Only the incident vortex Γ_0 is present; its trajectory is governed by equation (3.4) with $\Gamma \equiv 0$. The trajectory is depicted in Figure 2(a) for $d/h = \frac{1}{2}$, i.e. when the initial distance of the vortex from the wall is half the step height. The points labelled along the path indicate the vortex position at various nondimensional times Ut/h, where time is reckoned from the instant at which the vortex passes the step (at $x = 0$).

When $Ut/h \to -\infty$ (far from the step) the kinetic energy of the (incompressible) motion per unit length of the vortex is equal to $(\rho_0 \Gamma_0^2/4\pi)\ln(d/r_0)$, where r_0 is a length of the order of the radius of the vortex core (Lamb 1932). In the absence of shedding, this energy is conserved during interaction with the step, so that the distance of the vortex from the wall ultimately returns to d after the interaction when Ut/h becomes large. Because of this, the ratio Ut/h is approximately equal to the horizontal distance of the vortex from the step measured in step heights.

The nondimensional acoustic pressure

$$\frac{p(\mathbf{x}, t)}{\rho_0 U^2 M (d/h)^3 (\ell/|\mathbf{x}|)\cos\theta} \tag{3.8}$$

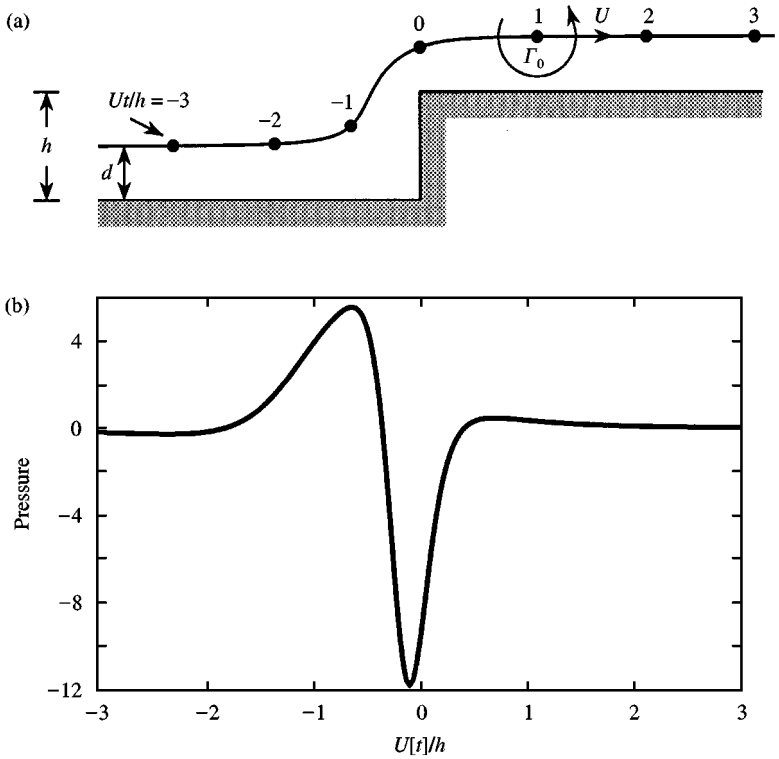

Figure 2. (a) Trajectory of the incident vortex in the absence of shedding for $d/h = 0{\cdot}5$. (b) Nondimensional acoustic pressure $p(\mathbf{x}, t)/[\rho_0 U^2 M (d/h)^3 (\ell/|\mathbf{x}|)\cos\theta]$; $[t] = t - |\mathbf{x}|/c_0$ denotes the retarded time.

is plotted in Figure 2(b) as a function of the nondimensional retarded time $U[t]/h$, $[t] = t - |\mathbf{x}|/c_0$. Most of the sound is generated just prior to the arrival of the vortex at the step, within a distance equal approximately to the step height h.

Figure 3 illustrates how this picture is dramatically changed when account is taken of separation at the step. The incident vortex path is deflected sideways by the shed vortex [Figure 3(a)], and the two vortices proceed away from the wall in a direction initially inclined towards negative x. The times indicated on the trajectories correspond to those in Figure 2, i.e. $t = 0$ defines the instant at which the vortex Γ_0 would pass over the step in the absence of shedding. The strength of the shed vortex increases as Γ_0 approaches the step until its value at $Ut/h = 1$ is about $-1{\cdot}2\Gamma_0$. More details of the variation of $\Gamma(t)$ are given

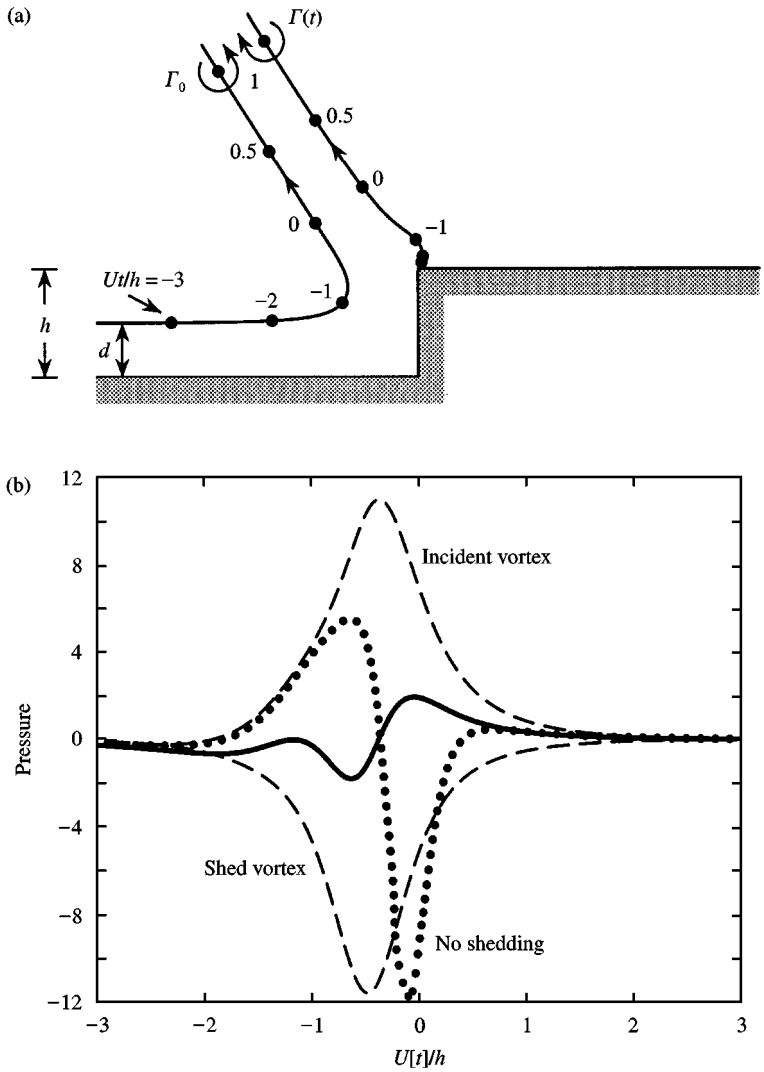

Figure 3. (a) Vortex trajectories when $d/h = 0{\cdot}5$. (b) ———, Nondimensional acoustic pressure $p(\mathbf{x}, t)/[\rho_0 U^2 M (d/h)^3 (\ell/|\mathbf{x}|)\cos\theta]$; ● ● ● ● ●, acoustic pressure in the absence of shedding. The broken curves are the separate contributions from the incident and shed vortices.

below. It should be noted, however, that, because $|\Gamma| > \Gamma_0$ when $Ut/h \geqslant 1$, the vortex pair traverses a circular path which ultimately causes the vortices to return to the wall and subsequently to separate at a "reattachment" point far to the right of the step. In more realistic flows, in particular in the presence of mean flow over the step in the x-direction, both the deflection distance away from the wall and the reattachment length would be much smaller.

The sound pressure produced by this interaction is represented by the solid curve in Figure 3(b). Also shown (dashed) are the acoustic pressures generated by the incident and shed vortices, which correspond, respectively, to the first and second terms in the square braces of equation (3.7). These separate contributions are both large, but of opposite sign, and interfere to produce a net radiated sound pressure that is much weaker than in the absence of shedding (shown dotted).

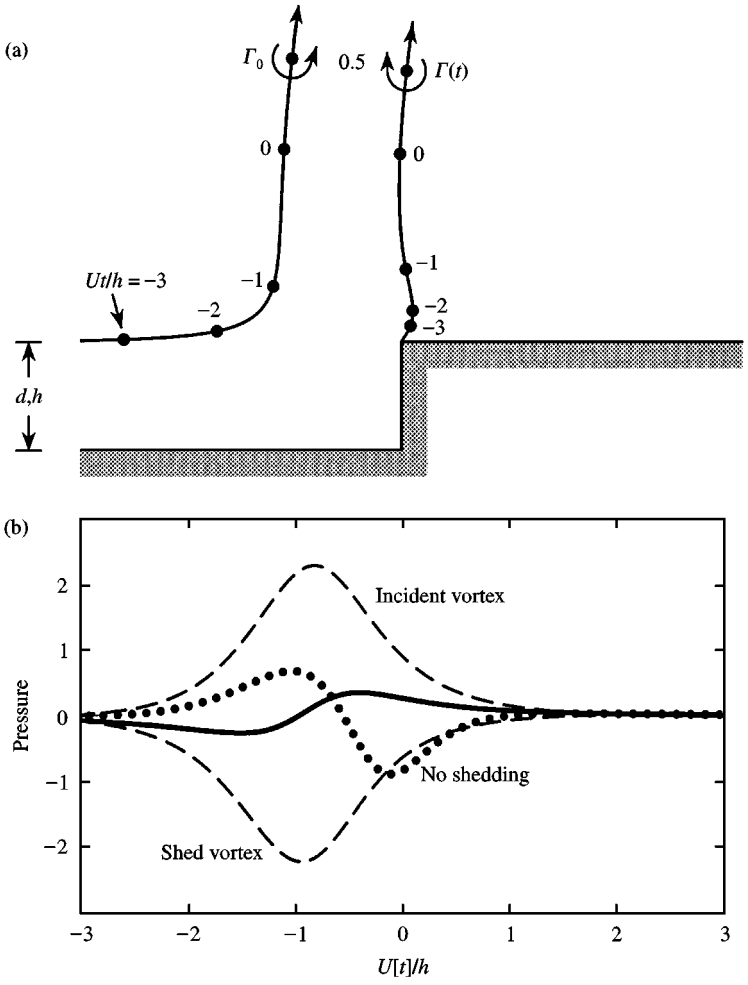

Figure 4. (a) Vortex trajectories when $d/h = 1$. (b) ———, Nondimensional acoustic pressure $p(\mathbf{x}, t)/[\rho_0 U^2 M (d/h)^3 (\ell/|\mathbf{x}|)\cos\theta]$; ● ● ● ● ●, acoustic pressure in the absence of shedding. The broken curves are the separate contributions from the incident and shed vortices.

When the initial stand-off distance of Γ_0 increases to $d = h$, Figure 4 shows that the trajectories and the pressure signatures are qualitatively similar to those of Figure 3; the acoustic amplitudes with and without vortex shedding are weaker, and the amplitude difference is smaller. If the vortex is assumed to be a crude model of a discrete eddy in a turbulent boundary layer, a larger value of d/h would be representative of turbulent flow over a small skin step, when the boundary-layer thickness tends to be large compared to h. The case in which $d/h = 4$ is illustrated in Figure 5. Here the deflection of the incident vortex is relatively small (about three step heights), and the circular path of the vortex pair terminates just to the right of the step (near $Ut/h \approx 3$), the trajectory being reminiscent of reattachment profiles observed in experiments (Farabee & Casarella 1984, 1986, 1988): the "eddy" formed by the vortex pair is torn apart, Γ_0 proceeding to the right along the wall and away from the step, while Γ is captured within a "separation bubble". Actually, $\mathrm{d}\Gamma/\mathrm{d}t$ changes sign at $Ut/h \approx 5{\cdot}2$, at which time it is "released" from the edge S with a final circulation $\Gamma = -1{\cdot}27\Gamma_0$. The vortex then proceeds back towards the step and proper continuation of the calculation requires that a new vortex be released from S. However, this latter phase of the motion will not be pursued (being similar to the interactions discussed below for the backward-facing step), since the interaction of the incident vortex Γ_0 with the

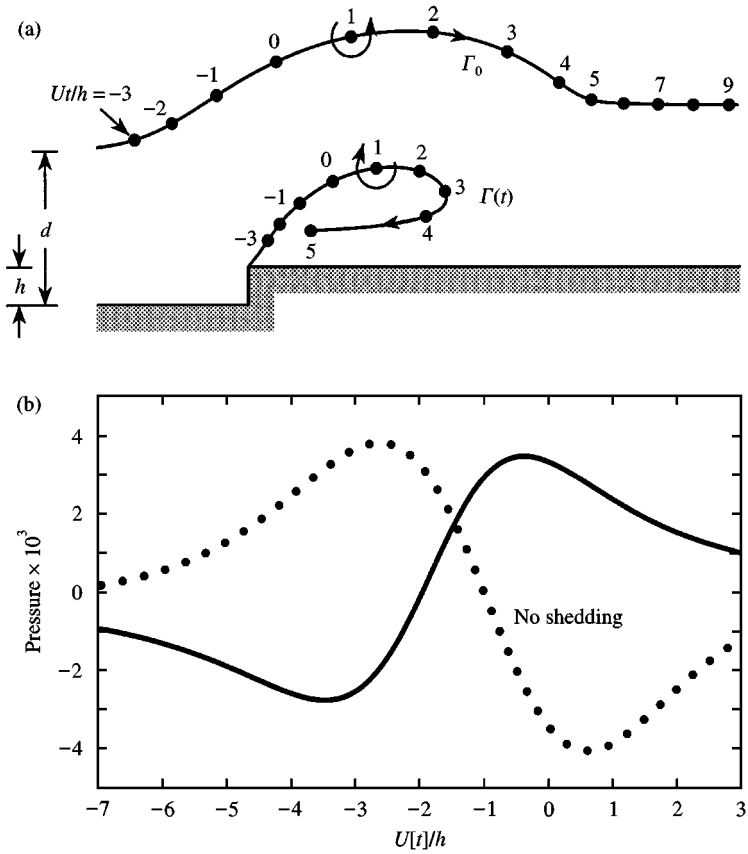

Figure 5. (a) Vortex trajectories when $d/h = 4$. (b) ———, Nondimensional acoustic pressure $p(\mathbf{x}, t)/[\rho_0 U^2 M(d/h)^3(\ell/|\mathbf{x}|)\cos\theta]$; ● ● ● ● ●, acoustic pressure in the absence of shedding.

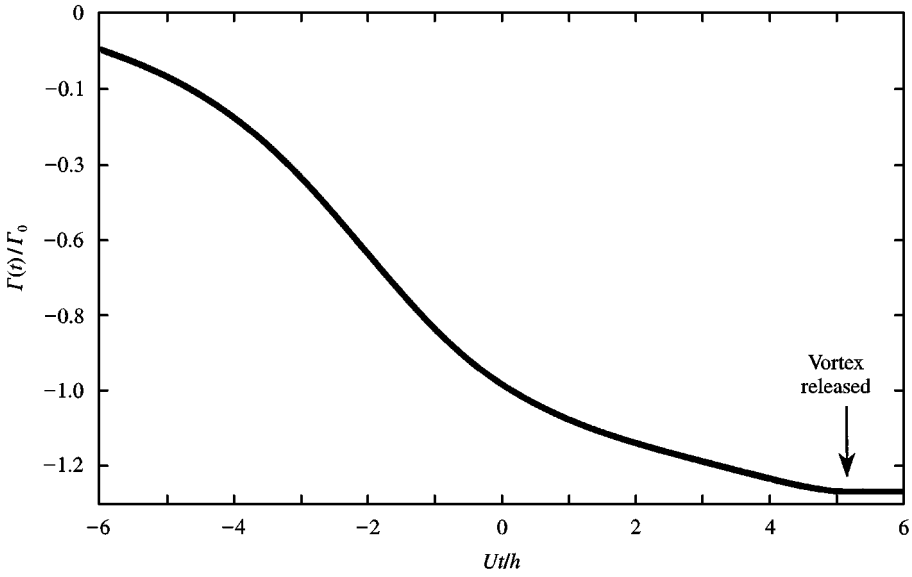

Figure 6. Shed vortex strength $\Gamma(t)/\Gamma_0$ for a forward-facing step when $d/h = 4$. The vortex is "released" from the edge S of the step at $Ut/h \approx 5{\cdot}2$.

step is now complete. The acoustic pressures with and without vortex shedding are seen in Figure 5(b) to be of very similar amplitude, but practically opposite in phase.

The variation of $\Gamma(t)/\Gamma_0$ when $d/h = 4$ is shown in Figure 6. The vortex is released at $Ut/h \approx 5{\cdot}2$ as indicated. In all of these cases, the sound is generated principally over an interval of time $\sim h/U$, with characteristic wavelength $\sim h/M \gg h$ at the small Mach numbers for which the present theory is applicable.

3.4. The Backward-Facing Step

Typical interactions for a backward-facing step are illustrated in Figures 7 and 8, respectively, for $d/h = 0{\cdot}5$ and 2. In the absence of shedding, the vortex paths and the acoustic pressure signatures are identical to their respective counterparts for the forward-facing step when the time direction is reversed. This is because of our assumption that the span ℓ of the wall "wetted" by the unsteady flow is small compared to the acoustic wavelength. As $\ell \to \infty$, an observer at a given far-field point $\mathbf{x}$ first receives sound from the interaction of the vortex and step occurring at the closest point of the step (corresponding essentially to the pressures calculated in this paper), but this is subsequently augmented at progressively increasing values of the retarded time with sound generated by interactions at increasing spanwise distances on the step from the observer.

When vortex shedding occurs at a backward-facing step, the incident vortex is displaced temporarily away from the wall [cf. Figures 7(a, b) and 8(a)], thereby reducing the intensity of the generated sound. The incident and shed vortex form a vortex pair (with $\Gamma \approx -\Gamma_0$ when $Ut/h \approx 1$) whose circular trajectory approaches the wall "downstream" of the step, where the pair split up as the flow "reattaches". The incident vortex continues along a path parallel to the wall and the shed vortex translates back towards the step within the

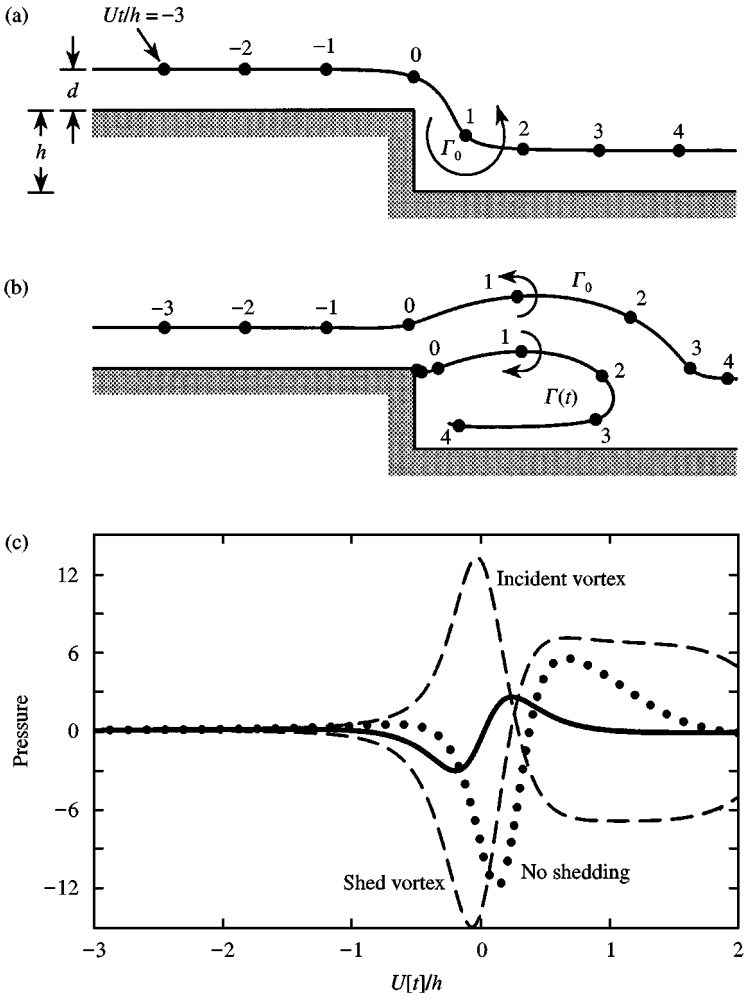

Figure 7. (a) Vortex trajectory for $d/h = 0{\cdot}5$ with no shedding. . (b) Trajectories with shedding. (c) ———, Nondimensional acoustic pressure $p(\mathbf{x}, t)/[\rho_0 U^2 M(d/h)^3(\ell/|\mathbf{x}|)\cos\theta]$; ● ● ● ● ●, acoustic pressure in the absence of shedding.

separation "bubble". This vortex is "released" before reaching the step (respectively, at $Ut/h \approx 2{\cdot}8$ oand $2{\cdot}2$ in Figures 7 and 8), whereupon a new vortex must be regarded as shed from S in order to continue the calculation. This secondary shedding has not been modelled because it occurs long after the interaction of Γ_0 with the step, and is probably not important in practice, since at these times surface interactions would be dominated by other dissipative mechanisms within the separation zone.

When $d/h = 0{\cdot}5$ the acoustic pressure (Figure 7) is much smaller than in the absence of shedding, and is "phase-advanced" with respect to the no-shedding pressure signature. The separate contributions to the radiation from the incident and shed vortices are again both large, but of opposite sign, and their interference determines the amplitude of the sound. Figure 8 shows that (in contrast to the forward-facing step) an increase in the initial stand-off distance to $d = 2h$ leaves the relative amplitudes of the acoustic pressures with and

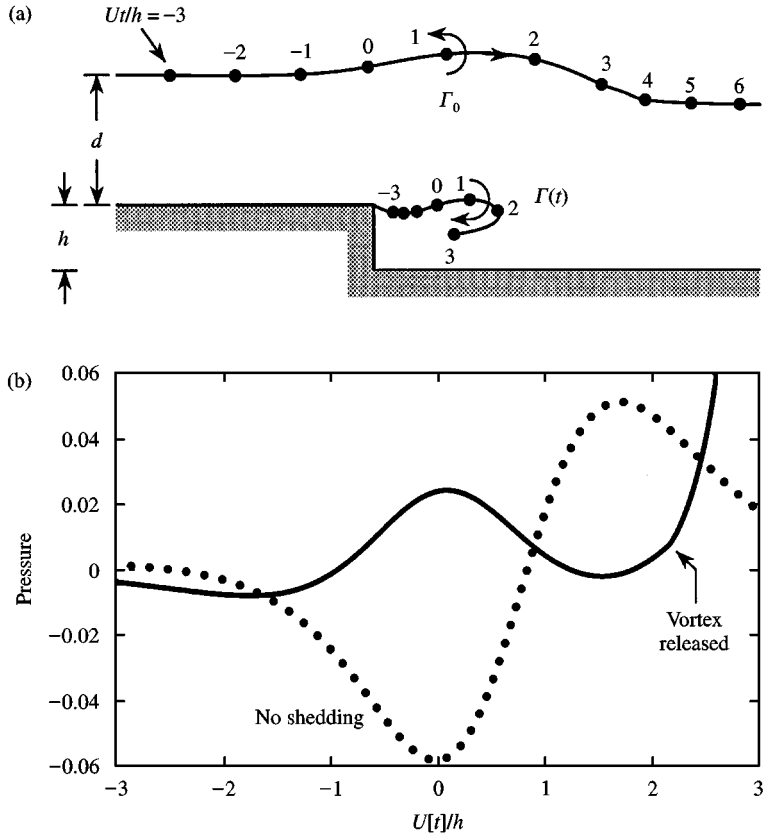

Figure 8. (a) Vortex trajectories when $d/h = 2$. (b) ———, Nondimensional acoustic pressure $p(\mathbf{x}, t)/[\rho_0 U^2 M(d/h)^3(\ell/|\mathbf{x}|)\cos\theta]$; ● ● ● ● ●, acoustic pressure in the absence of shedding.

without shedding effectively unchanged until the shed vortex is released. The subsequent sharp increase in the radiation after the release of the shed vortex at $Ut/h \approx 2{\cdot}2$ is of no practical significance, because it represents the sound generated when Γ returns to the step with no additional shedding from the corner.

4. CONCLUSIONS

The unsteady drag exerted on a stationary body in incompressible flow can be expressed entirely in terms of the vorticity distribution. To calculate drag fluctuations produced by impinging turbulence, it is important to include contributions from vorticity generated at the surface of the body. At low Mach numbers, the drag is equal to the strength of the aeroacoustic dipole that dominates the acoustic radiation. The numerical results given in this paper for an idealized vortex–step interaction suggest that vorticity in the separation zone significantly modifies the radiation compared to predictions based on a potential flow "edge scattering" modelling of the surface-generated sound. This may be representative of the kind of interaction that occurs when a large-scale, turbulent structure convects over forward or backward steps.

TABLE 1
Attenuation of vortex–step interaction noise by vorticity production

d/h	Attenuation (dB) Forward step	Backward step
0·1	11·8	10·1
1	6·3	9·7
2	3·5	9·0
4	1·4	4·8

The influence of shedding from a step of height h depends on the stand-off distance d of the vortex from the wall prior to the interaction. Predictions for large or small values of d/h might be expected to be relevant to sound production by turbulent flow over a step when the corresponding ratio δ/h of the boundary-layer thickness δ to the step height is large or small. Vorticity production affects both the amplitude and the phase of the sound. An overall estimate of the *attenuation* of the step noise by the surface-generated vorticity can be made by comparing the respective net-radiated acoustic energies $\mathscr{E}_s$ and $\mathscr{E}_o$, say, with and without vortex shedding. This is done by comparing corresponding values of $\int_{\infty}^{t_{max}} p^2(\mathbf{x}, t)\mathrm{d}t$, where the interaction of the step with the incident vortex is regarded as being negligible beyond a "cut-off" time t_{max}, which is introduced to eliminate large amplitude contributions from secondary interactions of the shed vorticity with the step (that are suppressed in practice by viscous dissipation and additional vorticity production at the wall). This comparison is made in Table 1, where the attenuation $-10\times\log_{10}(\mathscr{E}_s/\mathscr{E}_o)$ (dB) is given for several values of d/h. The attenuation decreases with increasing d/h ("boundary-layer thickness"), but less so for the backward-facing step, indicating that "reattachment" on top of a forward-facing step is noisier for a given value of d/h.

For a forward-facing step, when d/h is large, Figure 5 and Table 1 indicate that the amplitudes of the sound with and without shedding are roughly equal, but the phases are reversed; phase reversal is also evident in Figure 8 for the backward-facing step. These results suggest that predictions of the frequency spectrum of rough-wall boundary-layer noise based on the *potential flow scattering* of the turbulence blocked pressure by very small roughness elements [see e.g., Howe (1989b)] are probably satisfactory for practical purposes, and justifies in addition recent estimates of the noise generated by turbulent flow over small fuselage *skin steps* (Howe 1997).

ACKNOWLEDGEMENT

The work reported here is supported under Grant NAG1-1688 from NASA Langley Research Center, administered by Dr Richard J. Silcox.

REFERENCES

BRADSHAW, P. & WONG, F. Y. F. 1972 The reattachment and relaxation of a turbulent shear layer. *Journal of Fluid Mechanics* **52**, 113–135.

BROWN, C. E. & MICHAEL, W. H. 1954 Effect of leading edge separation on the lift of a delta wing. *Journal of the Aeronautical Sciences* **21**, 690–706.

Brown, C. E. & Michael, W. H. 1955 On slender delta wings with leading-edge separation. NACA Technical Note 3430.

Chandrsuda, C. & Bradshaw, P. 1981 Turbulent structure of a reattaching mixing layer. *Journal of Fluid Mechanics* **110**, 171–179.

Conlisk, A. T. & Veley, D. 1985 The generation of noise in impinging vortex motion past a step. *Physics of Fluids* **28**, 3004–3012.

Dhanak, M. R. & Gundlapalli, R. 1992 Flow noise due to interaction between an eddy and a forward facing step. In *Proceedings International Symposium of Flow Induced Vibration and Noise* Volume 3: *Flow–Structure and Flow-Sound Interactions* (eds T. M. Farabee & M. P. Païdoussis), pp. 11–22. New York ASME.

Eaton, J. K. & Johnston, J. P. 1981 A review of research on subsonic turbulent flow reattachment. *American Institute of Aeronautics and Astronautics Journal* **19**, 1093–1100.

Efimtsov, B. M. 1996 Non-homogeneous boundary layer noise prediction. Paper Presented at the NASA Langley Interior Noise Workshop, Hampton, VA, 10–12 September.

Farabee, T. M. & Casarella, M. J. 1984 Effects of surface irregularity on turbulent boundary layer wall pressure fluctuations. *ASME Journal of Vibration, Stress and Reliability in Design* **106**, 343–350.

Farabee, T. M. & Casarella, M. J. 1986 Measurements of fluctuating wall pressure for separated/reattached boundary layer flows. *ASME Journal of Vibration, Stress and Reliability in Design* **108**, 301–307.

Farabee, T. M. & Casarella, M. J. 1988 Wall pressure fluctuations beneath a disturbed turbulent boundary layer. In *Acoustic Phenomena and Interaction in shear flows over compliant and Vibrating Surfaces*, (eds, W. L. Keith, E. M. Uram & A. J. Kalinowski), pp. 121–135. New York: ASME.

Howe, M. S. 1975 Contributions to the theory of aerodynamic sound, with application to excess jet noise and the theory of the flute. *Journal of Fluid Mechanics* **71**, 625–673.

Howe, M. S. 1989*a* On unsteady surface forces, and sound produced by the normal chopping of a rectilinear vortex. *Journal of Fluid Mechanics* **206**, 131–153.

Howe, M. S. 1989*b* Sound produced by turbulent boundary layer flow over a finite region of wall roughness, and over a forward facing step. *Journal of Fluids and Structures* **3**, 83–96.

Howe, M. S. 1995 On the force and moment exerted on a body in an incompressible fluid, with application to rigid bodies and bubbles at high and low Reynolds numbers. *Quarterly Journal of Mechanics and Applied Mathematics* **48**, 401–426.

Howe, M. S. 1996 Emendation of the Brown and Michael equation, with application to sound generation by vortex motion near a half plane. *Journal of Fluid Mechanics* **329**, 89–101.

Howe, M. S. 1997 On the contribution from skin steps to boundary-layer generated interior noise. *Journal of Sound and Vibration* (in press).

Lamb, H. 1932 *Hydrodynamics* 6th edn; reprinted 1994. Cambridge: Cambridge University Press.

Moss, W. D. & Baker, S. 1980 Re-circulation flows associated with two-dimensional steps. *Aeronautical Quarterly* **39**, 151–172.